



ELSEVIER

Available online at [www.sciencedirect.com](http://www.sciencedirect.com)

SCIENCE @ DIRECT®

Nuclear Instruments and Methods in Physics Research A 527 (2004) 35–40

**NUCLEAR  
INSTRUMENTS  
& METHODS  
IN PHYSICS  
RESEARCH**  
Section A

[www.elsevier.com/locate/nima](http://www.elsevier.com/locate/nima)

# Methods to extract more light from minute scintillation crystals used in an ultra-high resolution positron emission tomography detector

Craig S. Levin\*, Frezghi Habte, Angela M. Foudray

*Stanford University School of Medicine, Department of Radiology, Division of Nuclear Medicine and Molecular Imaging Program,  
300 Pasteur Drive, Edwards Bldg. Rm. R354, Stanford, CA 94305-5344, USA*

## Abstract

Recently, there has been great interest in developing finely pixellated position-sensitive scintillation detectors for ultra-high-resolution Positron Emission Tomography (PET) systems designed for breast cancer detection, diagnosis, and staging and for imaging small laboratory animals. We are developing a different high-resolution PET detector design that promotes nearly complete scintillation light collection in  $\leq 1$  mm wide,  $> 10$  mm thick lutetium oxyorthosilicate (LSO) crystals. The design requires the use of semiconductor photodetector arrays in novel configurations that significantly improve the light collection aspect ratio for minute crystals. To reduce design complexity and dead area we are investigating the use of 1 mm thick sheets of LSO in addition to discrete crystal rods, and the use of position-sensitive avalanche photodiodes (PSAPDs) which require only four readout channels per device, in addition to pixellated APD arrays. Using a 1 mm thick scintillation crystal sheet coupled to a finely pixellated APD array results in a pseudo-discrete response to flood irradiation: due to a very narrow light spread function in the thin sheet we observe sharp ( $< 1$  mm wide) peaks in sensitivity centered at the APD pixel locations in a very linear fashion all the way out to the crystal edge. We measured an energy resolution of 13.7% FWHM at 511 keV for a 1 mm LSO crystal coupled to two APD pixels. Using a 1 mm thick crystal sheet coupled to a PSAPD the response to flood and edge-on irradiation with a  $^{22}\text{Na}$  point source shows a compressed dynamic range compared to that observed with discrete crystals or direct X-ray irradiation. With a discrete LSO crystal array the flood response is peaked at the crystal location where light is focused onto one spot on the PSAPD. We observed strong pin-cushioning effects in all PSAPD measurements. All LSO-PSAPD configurations studied had high aspect ratio for light collection and achieved energy resolutions  $\leq 12\%$  FWHM at 511 keV.

© 2004 Elsevier B.V. All rights reserved.

PACS: 87.59.-e; 87.59.Vb; 29.40.Mc

Keywords: High-resolution PET; Breast imaging; Small animal PET; Avalanche photodiode; Scintillation light collection

## 1. Introduction

Recently, there has been great interest in developing finely pixellated position-sensitive scintillation detectors for ultra-high-resolution

\*Corresponding author. Tel.: +1-650-736-2598; fax: +1-650-736-0234.

E-mail address: [clevin@stanford.edu](mailto:clevin@stanford.edu) (C.S. Levin).

Positron Emission Tomography (PET) systems designed for breast cancer detection, diagnosis, and staging and for imaging small laboratory animals [1–7]. The conventional approach to building a high-resolution PET detector uses an array of tiny crystal rods coupled end-on to a position-sensitive photodetector [1–7]. Extracting a significant fraction of the available light from the crystals in this manner proves to be difficult for 1 mm width crystal rods, especially since they should also be  $> 10$  mm long for adequate coincident photon detection efficiency [8]. We report some initial results obtained with novel ultra-high-resolution detector arrays we are investigating. The prototype detector utilizes lutetium oxyorthosilicate (LSO) crystal and new avalanche photodiode (APD) array designs that are placed in novel configurations that significantly improve the light collection aspect ratio [8]. These new design concepts promote nearly complete ( $> 95\%$ ) scintillation light collection with high (1 mm) intrinsic spatial resolution and at the same time high ( $> 82\%$ ) intrinsic 511 keV photon detection efficiency. To reduce design complexity and dead area, we are investigating the use of 1 mm thick sheets of LSO in addition to arrays of discrete crystal rods, and the use of position-sensitive APDs (PSAPDs) [8,9], that require only four readout signals, in addition to pixellated APD arrays [10]. The use of crystal sheets [11,12] and APDs [13–17] in PET have been investigated before, but not in the particular context or configurations presented in this work.

## 2. Methods

### 2.1. Configurations under investigation

Fig. 1 shows the high light collection configurations we are studying. Reading out the light from large faces of minute crystals rather than the narrow ends results in an order of magnitude greater light collection aspect ratio (ratio of crystal readout area to length).

The basic detector unit for study in this work is a single scintillation layer from the designs shown in Fig. 1 comprising a single scintillation crystal plane coupled to either a pixellated APD array or a PSAPD. Fig. 2 depicts two position sensing APD devices under investigation. Compared to unit gain semiconductor photodetectors APDs are appealing due to noise considerations. APD dark noise comprises parallel and series contributions. The major parallel noise sources are from the bulk and surface leakage currents of the device. The series component is a function of the device and input preamplifier capacitance. An expression for the rms dark noise for the device,  $\sigma_N^2$  expressed in terms of the number of electron–hole pairs created is given by [8]

$$\sigma_N^2 = 2e(I_B F + I_S/G^2)\tau + 4kTR_S(C_T^2/G^2)1/\tau \quad (1)$$

where  $e$  is the electron charge,  $I_B$  and  $I_S$  are the bulk and surface leakage currents, respectively,  $F$  is the APD excess noise factor,  $G$  is the device gain,  $\tau$  is the shaping time constant of the amplifier,  $k$  is

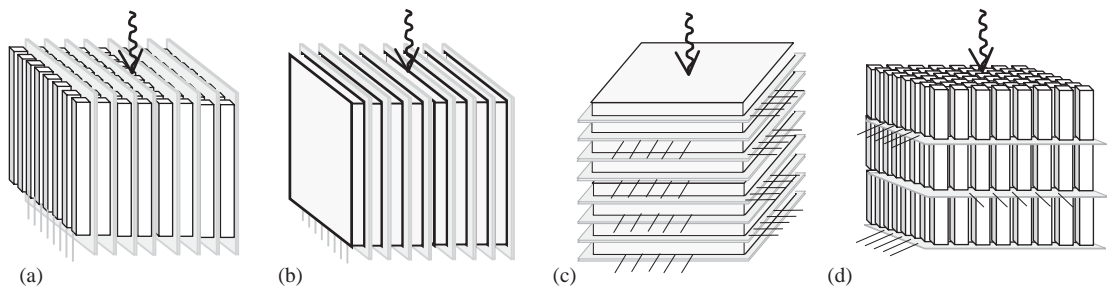


Fig. 1. Scintillation array configurations with high light collection efficiency under investigation. For high crystal packing fraction, the left two designs (a,b) require thin ( $\leq 300 \mu\text{m}$ ) APD arrays wedged between crystal planes and oriented edge-on with respect to incoming photons. The right two (c,d) configurations are face-on to incoming photons and do not require thin APD arrays, but for high inter-module packing fraction they require minute ( $\leq 300 \mu\text{m}$ ) dead space surrounding the sensitive area of the module. The far right design requires stacks of discrete crystal arrays, each  $\leq 3$  mm high for good light collection aspect ratio.

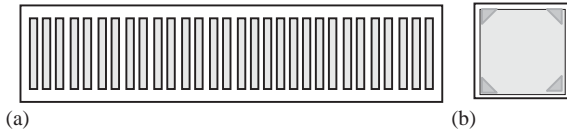


Fig. 2. Schematic drawings of two position sensing APD configurations we are studying for high light collection efficiency scintillation crystal imaging array designs. The left device (a) is a linear array of  $0.7 \times 7 \text{ mm}^2$  pixels on a 1 mm pitch spanning 4 cm, the right (b) “PSAPD” has a resistive anode surface with four corner readout electrodes and  $8 \times 8 \text{ mm}^2$  sensitive area. At the bias used the gain of this device is  $\sim 200$ , dark current  $\sim 50\text{--}100 \text{ nA}$ , capacitance per pixel  $\sim 3 \text{ pf}$ , and the dark noise  $\sim 30 \text{ e-rms}$ . The corresponding parameters for the PSAPD are 1000,  $1\text{--}2 \mu\text{A}$ ,  $45 \text{ pF}$ , and  $130 \text{ e-rms}$ .

the Boltzman constant,  $T$  the absolute temperature,  $R_s$  is the preamplifier series resistance, and  $C_T$  is the total preamplifier input capacitance from the APD and stray capacitance. In an APD the surface leakage current is not involved in the avalanche process. If the APD gain  $G$  is relatively high ( $> 200$ ), from Eq. (1) we see that the noise will be relatively low and dominated by the bulk leakage current term.

In the studies presented, the crystal layers and APDs are oriented either edge- or face-on with respect to incoming photons. We present only data for non-collimated  $^{22}\text{Na}$  (511 keV photon) irradiation of LSO crystal planes and  $^{55}\text{Fe}$  direct X-ray (5.9 keV) interactions in the silicon. For measurements with the pixellated line array (Fig. 2, left) a  $10 \times 7 \times 1 \text{ mm}^3$  (1 mm thick) LSO crystal sheet was coupled to nine array elements and flood irradiated with 511 keV annihilation photons from a  $^{22}\text{Na}$  source. Using the list mode data we formed a weighted mean of the digitized pulse heights for each scintillation event and plotted a 1D position histogram for this measurement. For studies with the PSAPD (Fig. 2, right) we used either a  $8 \times 8 \times 1 \text{ mm}^3$  LSO sheet or an array of discrete  $2 \times 2 \times 3 \text{ mm}^3$  LSO crystals. PSAPD events were positioned using the four corner anode signals in an Anger-type logic [9]. The pixellated array will be used to generate 1D histograms, the PSAPD will create 2D images. Energy spectra were fitted to a Gaussian superimposed on an exponential background to obtain full-width-at-half-maximum (FWHM) resolution values.

## 2.2. Data acquisition

For the pixellated arrays, the multiple APD array signals involved in each scintillation event are read out by an application specific integrated circuit (ASIC) (IDE AS, Norway), digitized, and sent to a PC in list mode. For the PSAPD measurement, the four anode corner signals involved in each scintillation event are read out by discrete charge sensitive preamplifiers (Cremat, Massachusetts) and NIM electronics, digitized, and sent to a Mac in list mode for processing. Note that for these studies we used commercially available front-end electronics that are not designed for the high-APD dynamic range (gains of 200–5000). This required us to implement AC coupling with  $> 1 \text{ M}\Omega$  terminating resistors, which severely attenuated the available charge signal, which thus somewhat degrades all results we report.

## 3. Results

Fig. 3 (left and middle) shows the results of  $^{22}\text{Na}$  flood irradiating the  $10 \times 7 \times 1 \text{ mm}^3$  crystal sheet coupled to the pixellated line array. Using a 1 mm thick crystal sheet coupled to a finely pixellated APD array results in a pseudo-discrete response to flood irradiation: Due to a very narrow ( $\sim 1 \text{ mm}$  FWHM) light spread function in the thin sheet and the APD pixellation, we observe sharp ( $< 1 \text{ mm}$  wide) peaks in sensitivity centered at the APD pixel locations in a very linear fashion all the way out to the crystal edge. Fig. 3 (right) shows a  $^{22}\text{Na}$  energy spectrum measured by coupling the  $1 \times 7 \text{ mm}^2$  edge of the  $10 \times 7 \times 1 \text{ mm}^3$  crystal to two APD pixels and summing the two signals. We measured 13.7% FWHM at 511 keV using a non-optimal 500 ns shaping time.

Fig. 4 shows the results of flood irradiating the  $8 \times 8 \text{ mm}^2$  PSAPD array using  $^{55}\text{Fe}$  X-rays without a crystal (left) and  $^{22}\text{Na}$  with a  $8 \times 8 \times 1 \text{ mm}^3$  LSO crystal (middle). This measurement is relevant for the face-on configuration depicted in Fig. 1c. The raw flood image data for the LSO sheet shows a compressed dynamic range compared to that observed for direct X-ray

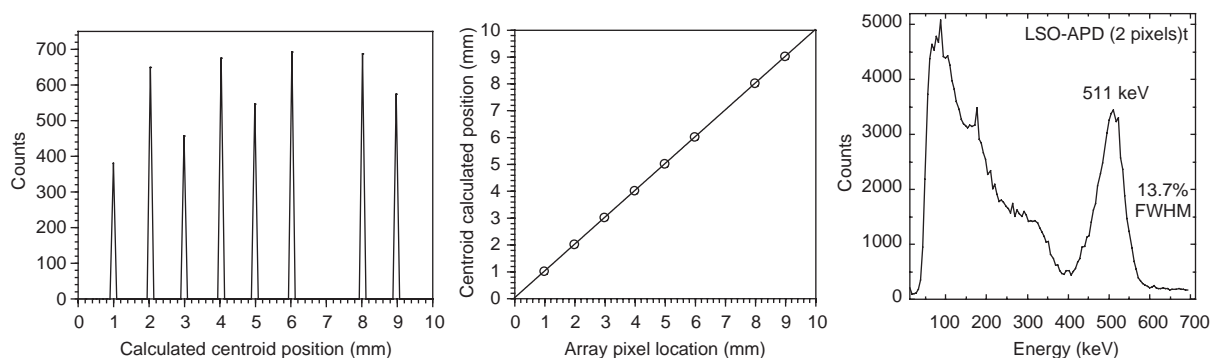


Fig. 3. Left:  $^{22}\text{Na}$  flood histogram results for  $10 \times 7 \times 1 \text{ mm}^3$  LSO crystal (1 mm thick) coupled to nine elements of the pixellated line array ( $0.7 \times 7 \text{ mm}^2$  pixels on a 1 mm pitch). Middle: Plot of calculated peak position vs. APD pixel location. Right: Measured  $^{22}\text{Na}$  energy spectrum using the same LSO crystal-coupled edge-on to two adjacent APD pixels with signals summed.

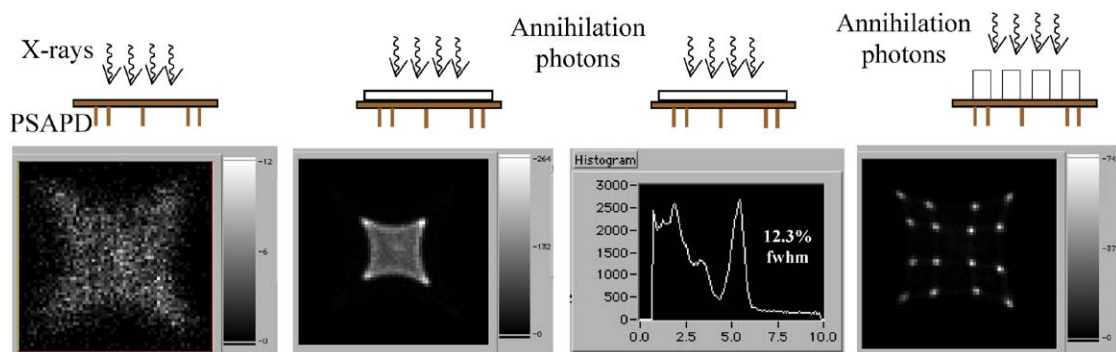


Fig. 4. PSAPD data relevant to face-on configurations (Figs. 1c,d) from left to right: 5.9 keV  $^{55}\text{Fe}$  direct X-ray interactions in silicon;  $^{22}\text{Na}$  511 keV photons on  $8 \times 8 \times 1 \text{ mm}^3$  LSO sheet; energy spectra measured from the latter; 511 keV photons on a  $4 \times 4$  array of  $2 \times 2 \times 3 \text{ mm}^3$  discrete crystals. The PSAPD has a  $8 \times 8 \text{ mm}^2$  sensitive area.

interactions. We measured 12.3% FWHM at 511 keV in the LSO sheet for flood irradiation. Fig. 4 (right) shows the results of 511 keV flood irradiation of a  $4 \times 4$  array of  $2 \times 2 \times 3 \text{ mm}^3$  LSO crystals. This latter measurement is relevant for the face-on detector configuration depicted in Fig. 1d. Note the dynamic range of the discrete crystal array data in Fig. 4 (right) is similar to that of the direct X-ray interactions (Fig. 4, left).

All PSAPD data shows the strong pin-cushioning effects due to non-linearity in charge sharing of the corner anodes across the face of the device. This pin-cushioning effect can be corrected for [9].

Fig. 5 shows the results of tests relevant to the edge-on detector designs depicted in Fig. 1a and b. Both a continuous sheet and discrete crystal array

were irradiated edge-on with 511 keV photons. For the latter the crystals were segmented lengthwise. In a full detector system this lengthwise segmentation would facilitate depth of interaction determination. The energy spectrum shown for the discrete crystal array represents the global sum over all crystals.

#### 4. Discussion

We are evaluating configurations of scintillation crystals that have high light collection aspect ratio in addition to high intrinsic spatial resolution and detection efficiency. In this report, we discussed preliminary results with a pixellated linear array

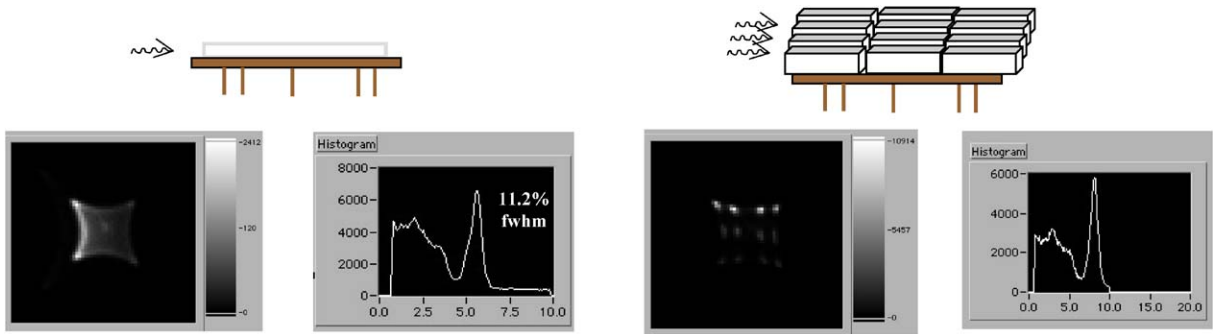


Fig. 5. PSAPD data relevant for edge-on configurations (Figs. 1a,b) from left to right: edge-on 511 keV irradiation of  $8 \times 8 \times 1 \text{ mm}^3$  LSO sheet; corresponding energy spectrum; edge-on 511 keV irradiation of a  $4 \times 3$  array of  $2 \times 2 \times 3 \text{ mm}^3$  discrete crystals; corresponding global energy spectrum over all crystals.

(Fig. 2a) and a position-sensitive APD (Fig. 2b). Flood irradiation of a 1 mm thick crystal sheet coupled to the pixellated array resulted in sharp peaks centered on the APD pixel locations (Fig. 3). This semi-discrete nature is analogous to and an extreme case of what happens in an Anger Camera if there is insufficient light diffusion from the crystal slab to the PMT array: positioned activity in a flood field image concentrates at the PMT centers. Note that the peaks seen correspond to the APD pixel locations and so there is excellent spatial linearity and dynamic range out to the crystal edge (Fig. 3 middle). These results indicate that the intrinsic spatial resolution for this 1D prototype using crystal sheets is roughly 1 mm and events could be positioned in 1 mm bins. A drawback of using this highly pixellated APD array design as it stands is that it requires many readout channels and an ASIC, which increases complexity. In addition, for a sheet crystal design, since the APD array is fairly insensitive between pixels, it follows we could be losing a significant amount of light and a configuration comprising one–one coupling of discrete crystals to individual APD elements as depicted in Fig. 1a might yield the best results.

The PSAPD generated some very interesting results. For direct X-ray irradiation the charge is created at discrete points in the silicon and the positioning dynamic range using the Anger-type positioning logic is good. The same is true for the discrete crystal array configurations we studied

that inject light into one concentrated spot on the PSAPD. However, for the 1 mm thick LSO sheet crystal, even though the FWHM of the light distributions are  $\leq 1 \text{ mm}$  [8], the tails of the light distribution produce a relatively wide distribution of charge deposited in the PSAPD, resulting in smaller differences between the corner anode signals. This is the cause of the compressed dynamic range observed in Fig. 4 (middle). We suggested using crystal sheets instead of discrete crystals to reduce complexity in manufacturing the detector arrays designs proposed. However, it is clear that for optimal results for the crystal sheet approach using a PSAPD it is necessary to investigate alternative, more intelligent positioning algorithms other than simple Anger-type logic [11].

For the pixellated design of Fig. 1d to have a high aspect ratio for light collection, the individual crystals should be short and many layers (perhaps more than three as shown) are required for high detection efficiency. This could significantly increase design complexity, but the corresponding imaging results for this configuration demonstrated the highest dynamic range.

Although the dynamic range of the edge-on discrete crystal array data (relevant to the designs of Fig. 1a or Fig. 5 top, right) was similar to that for the crystal sheet, the crystal segments could all be clearly identified. Of detector configurations studied with the PSAPD this discrete approach might represent the best compromise between simplicity in construction and unambiguous

localization of 511 keV photon interactions for an LSO–PSAPD scintillation detector. Note that due to the high light collection aspect ratios studied, and the continuous sensitivity of the PSAPD our measured energy resolutions were consistently at or below 12% FWHM at 511 keV.

The energy spectra presented for the discrete crystal configurations studied in this report were global sums over all crystals. Because of inter-crystal variations and variations in quantum efficiency and signal generation across the PSAPD face, individual rather than global crystal energy spectra will show superior resolution of the 511 keV photopeak. By position-gating on any given crystal in the image, the resulting energy spectra have been extracted and have demonstrated significantly improved resolution values over those quoted in this paper. We will report these values in a future study.

Note that for the studies presented we used commercially available front-end electronics that were not designed for the high APD dynamic range (gains of 200–5000). This required us to implement AC coupling with  $>1\text{ M}\Omega$  terminating resistors, which severely attenuates the available charge signals. We are currently developing dedicated readout electronics with an appropriate input dynamic range to improve upon the results presented.

### Acknowledgements

The authors would like to thank Dr. Kanai Shah, Richard Farrell, and Mickel McClish at RMD, Inc. for useful discussions and for providing APD samples. This work was supported by grants from the Susan G. Komen Foundation and National Institutes of Health (EB 003283 and CA 098691).

### References

- [1] G. Di Domenico, A. Motta, G. Zavattini, A. Del Guerra, C. Damiani, V. Bettinardi, M.C. Gilardi, Nucl. Instr. and Meth. Phys. Res. 477 (2002) 505.
- [2] J. Seidel, J.J. Vaquero, J. Pascau, M. Desco, 2002 IEEE International Symposium on Biomedical Imaging, 2002, p. 545.
- [3] J.A. Correia, C.A. Burnham, D. Kaufman, A.J. Fischman, 2001 IEEE Nuclear Science Symposium Conference Record, 2002, p. 1550.
- [4] M. Rafecas, G. Boning, B.J. Pichler, E. Lorenz, M. Schwaiger, S.I. Ziegler, 2001 IEEE Nuclear Science Symposium Conference Record, 2002, p. 1128.
- [5] G. Tzanakos, N. Apostolou, X. Benetou, G. Karmaniolas, G. Kontaxakis, M. Nikolaou, G. Panayotakis, S. Pavlopoulos, M. Skiadas, G. Spyrou, T. Thireou, 2000 IEEE Nuclear Science Symposium Conference Record, 2000, p. 21.
- [6] A. Chatziioannou, Y. Tai, Y. Shao, N. Doshi, B. Silverman, K. Meadors, S.R. Cherry, 2000 IEEE Nuclear Science Symposium Conference Record, 2000, p. 21.
- [7] R.S. Miyaoka, S.G. Kohlmyer, T.K. Lewellen, IEEE Trans. Nucl. Sci. NS-48 (2001) 1403.
- [8] C.S. Levin, IEEE Trans. Nucl. Sci. NS-49 (2002) 2236.
- [9] K.S. Shah, R. Farrell, R. Grazioso, E.S. Harmon, E. Karplus, IEEE Trans. Nucl. Sci. NS-49 (2002) 1687.
- [10] K.S. Shah, R. Farrell, R. Grazioso, R. Myers, L. Cirignano, IEEE Trans. Nucl. Sci. NS-48 (2001) 2352.
- [11] J. Joung, R.S. Miyaoka, T.K. Lewellen, 2001 IEEE Nuclear Science Symposium Conference Record, 2002, p. 1137.
- [12] S. Siegel, S.R. Cherry, A.R. Ricci, Y. Shao, M.E. Phelps, IEEE Trans. Nucl. Sci. NS-42 (1995) 1069.
- [13] Y. Shao, K. Meadors, R.W. Silverman, R. Farrell, L. Cirignano, R. Grazioso, K.S. Shah, S.R. Cherry, IEEE Trans. Nucl. Sci. NS-49 (2002) 649.
- [14] M. Rafecas, G. Boning, B.J. Pichler, E. Lorenz, M. Schwaiger, S.I. Ziegler, 2001 IEEE Nuclear Science Symposium Conference Record, 2002, p. 1128.
- [15] J. Liu, A. Fremout, P. Bruyndonckx, S. Tavernier, J.F. Loude, C. Morel, 2001 IEEE Nuclear Science Symposium Conference Record, 2002, p. 873.
- [16] R. Lecomte, C.M. Pepin, M.D. Lepage, J.F. Pratte, H. Dautet, D.M. Binkley, 2000 IEEE Nuclear Science Symposium Conference Record, 2000, p. 77.
- [17] P. Vaska, D.J. Schlyer, C.L. Woody, S.P. Stoll, V. Radeka, N. Volkow, 2001 IEEE Nuclear Science Symposium Conference Record, 2002, p. 1569.